Soils and Foundations 2013;53(1):117–129

The Japanese Geotechnical Society

Soils and Foundations

www.sciencedirect.com
journal homepage: www.elsevier.com/locate/sandf

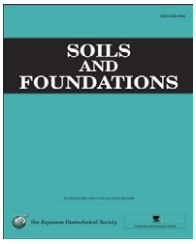

Centrifuge model tests of deformation and failure of nailing-reinforced slope under vertical surface loading conditions

Ga Zhang*, Jie Cao, Liping Wang

State Key Laboratory of Hydroscience and Engineering, Tsinghua University, Beijing 100084, PR China

Received 20 January 2012; received in revised form 15 July 2012; accepted 1 September 2012
Available online 1 February 2013

Abstract

A series of centrifuge model tests was conducted on a nail-reinforced slope under vertical surface loading conditions considering different slope gradients and nail lengths. The ultimate load of the slope decreased significantly with the increasing gradient of the slope or the decreasing nail length. The slope exhibited significant progressive failure that was captured by a displacement-based analysis. At first, the vertical load caused local slippage near the slope toe and the inner edge of the loading plate. Then, it extended to the interior of the slope and eventually to an entire slip surface. The *H-surface* was obtained according to the measured displacement to distinguish the zone where the surface load influenced the horizontal displacement of the slope. The *H-surface* and the position where the peak vertical displacement occurred in a horizontal line moved from the internal slope to the slope surface from the slope top to the slope bottom. This demonstrates the dispersion of the surface load application within the slope. The deflections of nails can be obtained from the corresponding soil deformation. The deflection of nails increased with the increasing load pressure, and exhibited diverse features in its distribution in the upper and the lower parts of the slope.

Keywords: Slope; Reinforced soils; Soil nailing; Failure; Centrifuge modelling (IGC: E06, E12, E14)

1. Introduction

Soil nails have been widely employed to improve the stability level of slopes as a cost-effective stabilising measure (e.g., Nowatzki and Samtani, 2004; Turner and Jensen, 2005). Methods based on the limit equilibrium or a limit analysis have usually been used in the design of soil–nailed structures (e.g., Shen et al., 1981; Juran et al., 1990), which are incapable of considering the soil–nail interaction reasonably. The finite element method and other types of numerical methods have also been developed or used to analyse the behaviour of nail-reinforced slopes (e.g., Kim et al., 1997; Yang and Drumm, 2000; Gui and Ng, 2006; Zhou et al., 2009).

The response of full-scale nailed slopes has been observed and measured in order to evaluate the safety levels of the slopes and to analyse their behaviour rules (e.g., Andrzej et al., 1988; Guler and Bozkurt, 2004; Turner and Jensen, 2005). As one of the most successful geotechnical laboratory techniques, centrifuge modelling has been widely used for studying the behaviour of reinforced slopes, since gravity-related deformation and failure can be

*Corresponding Author. Tel./fax: 86 10 62795679.
E-mail addresses: zhangga@tsinghua.edu.cn (G. Zhang), caojie.06@gmail.com (J. Cao), wlp04@mails.tsinghua.edu.cn (L.P. Wang).

Peer review under responsibility of The Japanese Geotechnical Society.

Production and hosting by Elsevier

0038-0806
http://dx.doi.org/10.1016/j.sandf.2012.12.008

simulated effectively (e.g., Zornberg et al., 1998; Zhang et al., 2001; Hu et al., 2010; Wang et al. 2011). Wang et al. (2010) performed centrifuge model tests to compare the response of nail-reinforced and unreinforced slopes under earthquake conditions. The nails were discovered to not only significantly decrease the deformation with more uniform distribution within the slopes, but also to arrest the possible failure that would occur in unreinforced slopes.

The footings have often been placed on different types of slopes, and have provided a surface load on the slopes. Thus, the surface loading conditions of slopes should be of concern. The bearing capacity of footings on slopes is usually significantly smaller than that of footings on the level ground, and therefore, the slopes have often been reinforced using different structures. A number of model tests and numerical analyses have been employed to study the behaviour of footings on reinforced slopes, including influence factors and failure mechanisms (e.g., Lee and Manjunath, 2000; Yoo, 2001; Alamshahi and Hataf, 2009; Sommers and Viswanadham, 2009). El Sawwaf (2005) conducted a series of laboratory model tests to investigate the behaviour, with the influence rules of different factors, of a strip footing on a sandy slope reinforced by a row of piles and a sheet pile.

Most of the previous investigations have focused on the limit bearing capacity of footings on slopes; however, very few researches have dealt with the deformation and the failure process of slopes. Significantly, the bearing capacity of a footing is often determined according to the settlement limit for deformation control. It should be recognised that evaluations of the bearing capacity of footings on slopes depends on the understanding of the deformation and the failure mechanism under surface loading conditions. Therefore, a systematic investigation is required on the deformation-failure behaviour of nail-reinforced slopes due to the application of surface loading. Centrifuge modelling is an effective approach for a thorough insight into the behaviour of nail-reinforced slopes under surface loading conditions, although such tests have hardly been conducted up to now.

In this study, a series of centrifuge model tests was conducted on a nail-reinforced slope under vertical surface loading conditions. The gradient of the slope and the nail length were varied to examine their effects on the response of the slope and of the nails. The response in the load–settlement relationship of the loading plate and the displacement of the slope was measured during the loading process. The deformation behaviour and the failure process of the slope were analysed using a displacement analysis and a strain analysis. In addition, the response of the nails was examined by measuring their deflections.

2. Description of model tests

2.1. Devices

The 50 g t geotechnical centrifuge at Tsinghua University, with a maximum acceleration of 250g, was used for the centrifuge model tests. The model container used for the tests was made of aluminium alloy, 500 mm in length, 200 mm in width, and 350 mm in height. A vertical loading device was installed at the top of the model container. This device can provide a vertical load with a capacity of 10 kN on the loading plate through the shaft, which was driven by an electric motor and a corresponding reducer (Fig. 1(a)). The loading rate was maintained during the tests and could be adjusted in advance of the tests. The loading plate consisted of a pair of steel plates with a few rolling contact bearings between them so that the horizontal friction between the loading plate and the soil could be eliminated and only the vertical load was applied to the top of the slope. The loading plate was 198 mm long in the orthogonal direction to the slope, which was

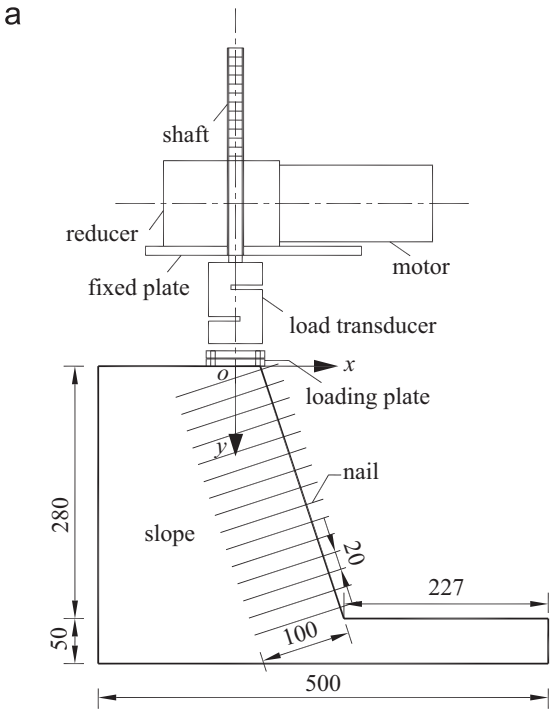

Fig. 1. Schematic views of test model for 3:1 slope with nail length of 100 mm. (a) Elevation view with loading device (unit: mm), (b) Image of slope model.

approximately equal to the width of the slope model. Therefore, the plane strain condition was assured during the tests. The loading plate was 65 mm in width for all the tests in this paper. The plate was rigidly connected to the loading shaft and the possible tilting of the loading plate was restricted by the loading system. In other words, the loading plate was kept horizontal during the loading, which was verified through observations after the tests.

2.2. Schemes

A series of centrifuge model tests was conducted on nail-reinforced slopes with the application of a vertical load on the top of the slope (Table 1). The tests simulated two main factors that influence the response of the slope and the nails, namely: (1) The gradient of the slope (Vertical: Horizontal) ranged from 1.5 to 5; (2) The nail lengths were 50 mm, 80 mm, and 100 mm.

2.3. Model preparation

Fig. 1 shows the schematic and the photographic views of the nail-reinforced model slope. The slope was 280 mm in height for all the tests, and a horizontal ground soil layer, 50 mm in depth, was set to reduce the influence of the model container. Silicone oil was painted on both sides of the container to reduce the friction with the slope.

The soil was retrieved from the soil base of a high building in Beijing. The specific gravity of the soil was 2.7. The plastic limit and the liquid limit of the soil were 15.5% and 33.5%, respectively. The dry density and the water content of the soil were controlled around 17% and 1.51 g/cm^3, respectively, for the centrifuge model tests. The shear strength of the soil was 26 kPa in cohesion and 24° in internal frictional angle. The soil was compacted into the container in layers, with a thickness of 50–60 mm, and the slope for the test was obtained by removing the redundant soil.

Thin steel needles in columniform were used to simulate the nails of the reinforced slope. The tensile strength and the elastic modulus of the steel were 200 MPa and 210 GPa, respectively, which were equivalent for the prototype and the model. The diameter of the needle was about 1 mm, equivalent to 50 mm at a centrifugal acceleration of 50g for a prototype nail. It should be noted that it would have been difficult to prepare the model sample if thinner steel needles had been used. The stiffness of the nail, at the prototype or model dimensions, can be derived accordingly. The nails were homogenously inserted into the slope with a spacing of 20 mm, perpendicular to the slope surface with a certain length outcropping the slope surface.

Table 1
List of centrifuge model tests.

No.	Slope gradient (V:H)	Nail length (mm)
1	2:1	100
2	2:1	50
3	3:1	100
4	3:1	80
5	3:1	50
6	5:1	100
7	1.5:1	100

The behaviour of the nail–soil interface, such as the surface roughness of the nail, was equivalent for the prototype and the model. A series of nail pull-out tests under different overburden pressures was conducted to determine the friction behaviour between the nail and the soil. In each test, the nail was pulled out from within the soil sample that was applied with a constant overburden stress. The friction stress around the nail, which was calculated according to the measured pull-out force, was discovered to be approximately proportional to the overburden pressure. Thus, according to the test results, the relationship between the friction stress and the overburden pressure can be described using the Mohr–Coulomb criterion with cohesion of 16 kPa and a frictional angle of 23°.

2.4. Test process and measurements

In each test, the centrifugal acceleration was increased gradually to the 50g-level. During the increase in centrifuge acceleration, the loading plate, which was fixed on the loading device, did not contact the top of the slope before the surface loading was applied. After the settlement at the top of the slope became stable, at the 50g-level, the vertical load was monotonically applied at rate of 1 mm/s. A load transducer was installed on the loading plate to measure its load at the top of the slope during the loading tests (Fig. 1(a)). The load pressure was further calculated by dividing the measured load by the area of the loading plate; the dimensions were equivalent for the model and the prototype. Only a laser displacement transducer was installed on the loading plate to measure its settlement, because the loading plate maintained its level during the loading tests (Fig. 1(a)).

An image-recording and displacement measurement system was used to record the images of the slope during the tests (Zhang et al., 2009). After picking out the measurement points and an image series, an image-correlation analysis algorithm, matching the image pattern of a small region around each measurement point between the two adjacent images, was selected. Through the corresponding positions of the measurements in different images, the displacement vectors for an arbitrary point on the lateral side of the slope could be obtained. A number of white granite particles were placed on the slope side for a colourful region with a significant grey scale difference to satisfy the measurement requirements (Fig. 1(b)).

The accuracy of the displacement measurement reached 0.03 mm at the model dimension. The Cartesian coordinate system was established with the centre of the loading plate as its origin. It was defined as positive downward in the vertical direction (y-axis), and to the right in the horizontal direction (x-axis) (Fig. 1(a)). The measured displacement was presented at the model dimension in this paper, which can be derived for the prototype dimension by multiplying the g-level used in the tests. The strain was equivalent for the model and the prototype dimensions.

3. Load–displacement relationship of loading plate

Fig. 2 shows the load–settlement relationship of the loading plate on the 3:1 slopes reinforced by nails with different lengths. It can be observed that the load pressure on the loading plate increased with a decreased rate as the settlement of the loading plate increased in all the tests during the initial loading period. The load pressure exhibited an evident decrease as the settlement of the loading plate increased beyond about 2.1 mm when the nail was 50 mm in length. On the other hand, the load pressure became nearly stable as the settlement of the loading plate increased when the nail lengths were 80 mm and 100 mm. This demonstrates that the nail length has a significant effect on the load–settlement relationship of the loading plate.

The ultimate load pressure of the slope was defined as the stable value or the peak value of the load pressure in the load–settlement curves, which is marked using solid points in Fig. 2. Fig. 3 compares the ultimate load pressure of the slope obtained from different tests. It can be seen that the ultimate load pressure of the slope decreased significantly with an increasing gradient of the slope or decreasing nail length.

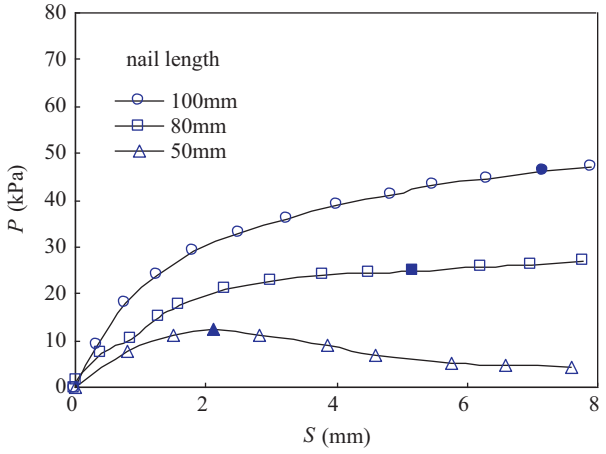

Fig. 2. Load–settlement curve for 3:1 slope reinforced by nails with different lengths at model dimension. P: load pressure on loading plate, S: settlement of loading plate, solid point, ultimate load pressure.

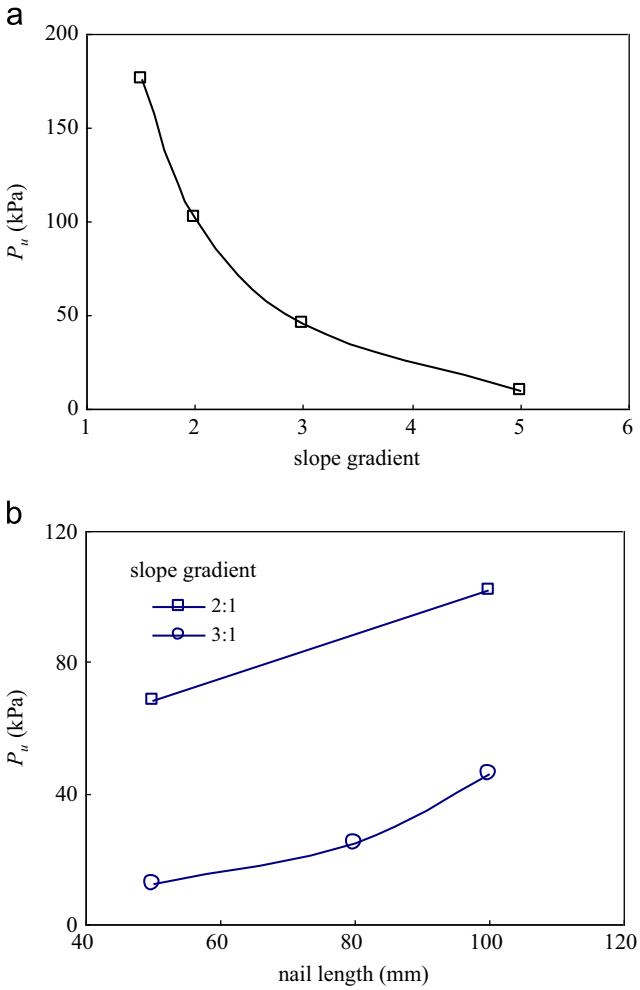

Fig. 3. Ultimate load pressure of slope in different tests at model dimension. P_u: ultimate load pressure. (a) Effect of slope gradient (nail length: 100 mm), (b) Effect of nail length.

4. Progressive failure of slope

Fig. 4(a) shows a photograph of the 3:1 slope reinforced with 100-mm-long nails after the test. Two slip surfaces were discovered from the photograph and outlined in Fig. 4(b). Close examination after the tests showed that the slip surfaces of the slope went through at the orthogonal direction from the front lateral side to the opposite side of the model; this demonstrates that the plane strain condition was valid. The slip surface nearly passed through the inner edge of the loading plate and the slope toe. The compression of the loading plate induced an evident punch body with a nearly triangular shape under the loading plate, and a secondary slip surface appeared subsequently. In addition, a vertical fracture surface occurred along the inner edge of the loading plate. Fig. 5 shows the displacement vectors of the 3:1 slope at different settlements of the loading plate. It can be seen that the displacement of the slope increased from the internal slope to the slope surface and decreased from the slope top to the slope bottom. The slip body can be distinguished according to the vectors' distribution at the loading plate settlement of

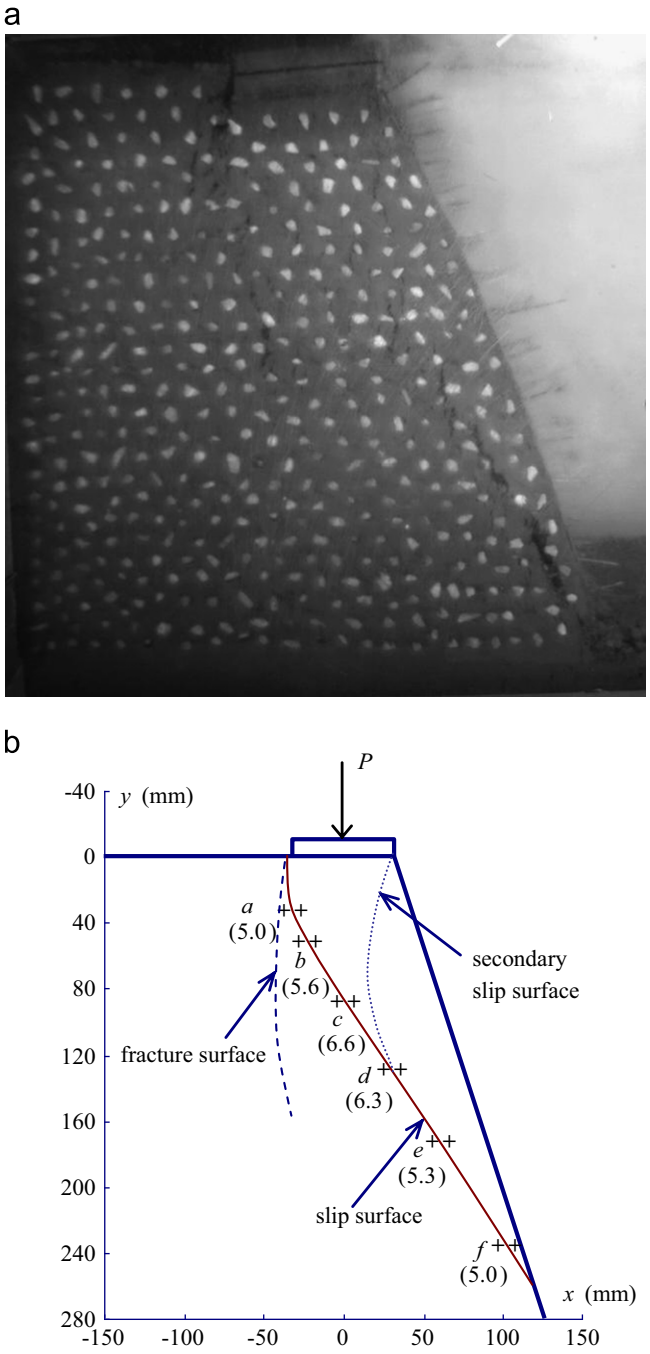

Fig. 4. Slip surface of 3:1 slope with nail length of 100 mm. Numbers in brackets show settlements of loading plate corresponding to appearance of slippage at model dimension (unit: mm). (a) Image, (b) Schematic view and point couples.

7 mm, at which the load pressure of the slope reached the ultimate value.

Fig. 6 compares the slip surfaces of the slope with different nail lengths or different slope gradients. The boundaries of the nail-reinforced zones are also outlined in the figure. The end points of these three slip surfaces were very close; this demonstrates that the surface load was the dominant factor to the slip surface. The nail length was also indicated to have an effect on the slip surface

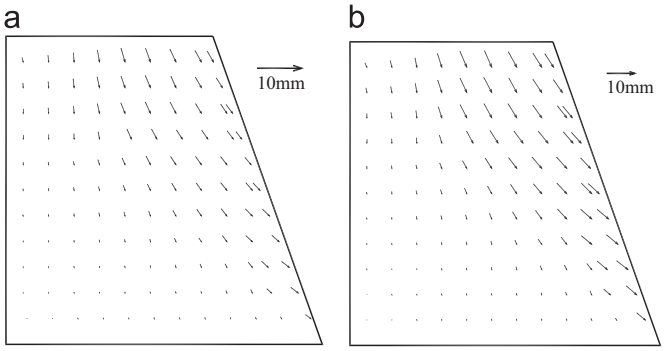

Fig. 5. Displacement vectors of 3:1 slope with nail length of 100 mm. (a) Settlement of loading plate: 4 mm, (b) Settlement of loading plate: 7 mm.

(Fig. 6(a)). The slip surface of the slope exhibited a backward tendency with a decreasing nail length so as to pass by the nails. For example, the slip surface was behind the nail-reinforced zone when the nail was 50 mm long, while it was entirely in the nail-reinforced zone when the nail length was 100 mm long. The slip surface was also affected by the slope gradient (Fig. 6(b)). The nail length should be determined according to the critical slip surface of the reinforced slope and was significantly dependent on the features of the surface load, which had not been reasonably considered in the currently existing nail design codes.

The failure process was investigated by analysing the relative displacement of the point couples alongside the slip surfaces. The point couple consisted of a pair of points that were located on opposite sides of the slip surface, with the spacing of 10 mm. Six groups of point couples were selected along the slip surface of the 3:1 slope with a nail length of 100 mm (Fig. 4(b)). The relative displacement between the couple of points in the tangential direction to the slip surface was obtained using the image-based measurement system (Fig. 7). It can be seen that the relative displacement of the point couples increased with an increasing settlement of the loading plate. An evident inflexion appeared in the history curves, which is marked using dashed lines in Fig. 7. The relative displacement exhibited a remarkable increase after the inflexion, demonstrating evident slippage between the point couples. Thus, this inflexion can be used to indicate the occurrence of local failure in the slope. Accordingly, the settlements of the loading plate, at which the local slippage appeared along the slip surface, were obtained and labelled in Fig. 4(b). It can be seen that the local failure occurred earlier near the top of the slope than in the middle of the slope. This is because the application of the surface load caused the displacement of the slope to concentrate at the inner edge of the loading plate via the loading plate with a limited width. Thus, the entire slip surface developed neither from the slope toe monotonically to the slope top nor in the opposite direction. The failure process of the slope can be described as follows. The vertical load caused local slippage near the slope toe and the inner edge of the

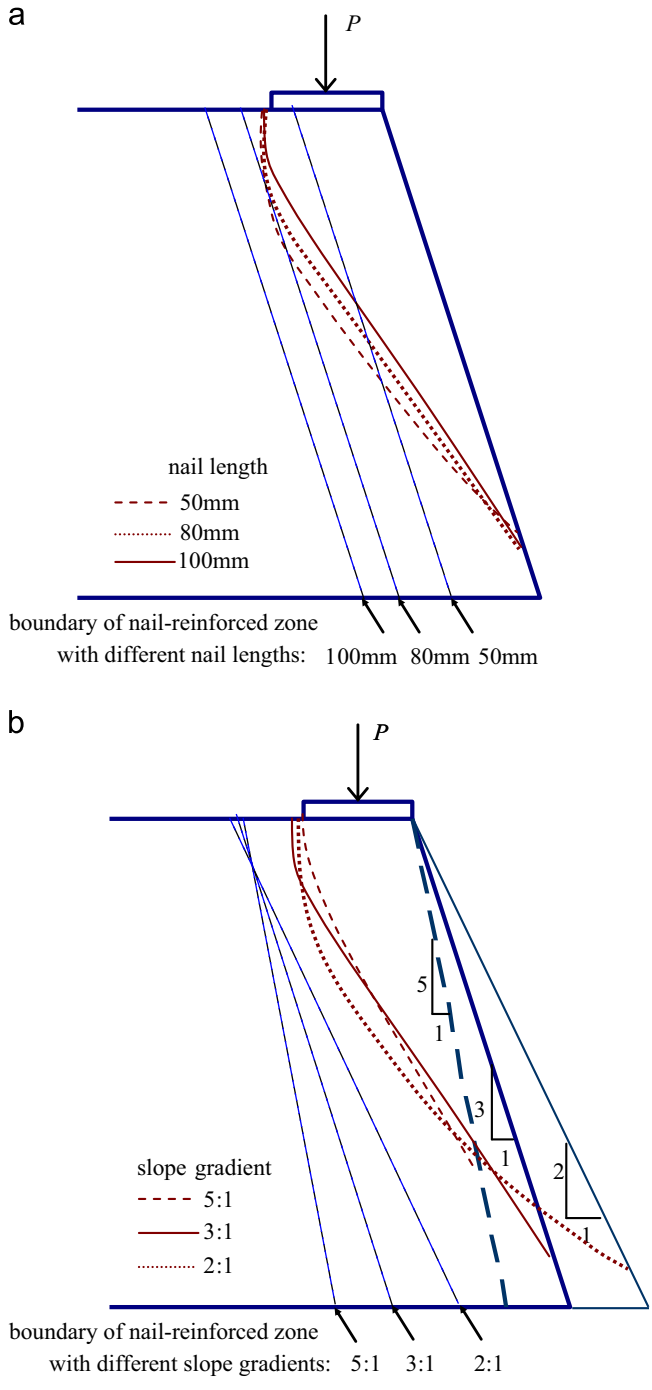

Fig. 6. Slip surface of slope in different tests. (a) 3:1 slope with different nail lengths, (b) Slopes with different gradients (nail length: 100 mm)

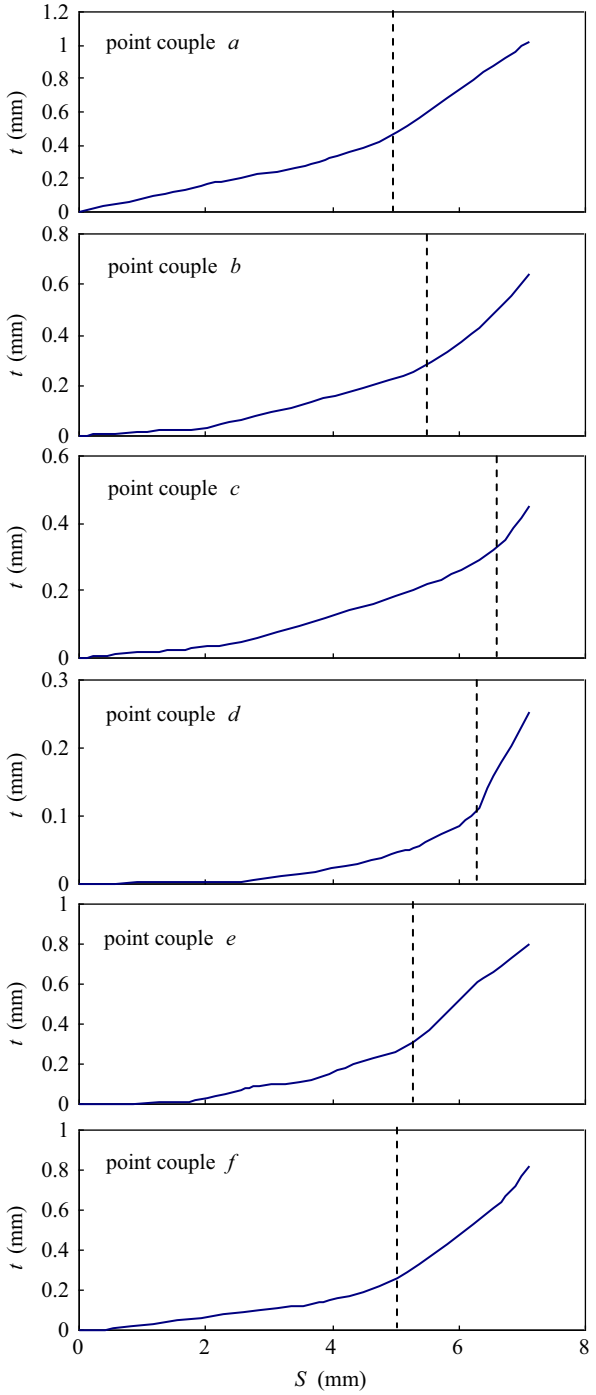

Fig. 7. Histories of relative displacement of point couples of 3:1 slope with nail length of 100 mm at model dimension. t: relative displacement tangential to slip surface, S: settlement of loading plate.

loading plate at first. These local slippages extended to the interior of the slope and eventually developed to an entire slip surface. This demonstrates that the nail-reinforced slope performed a significant progressive failure. The stability analysis of reinforced slopes should capture the effect of progressive failure, which cannot be considered by the commonly-used limit equilibrium methods.

Fig. 8 further shows the failure processes of the 3:1 slope with nail lengths of 80 mm and 50 mm. Close examination of Fig. 4(b) and Fig. 8 indicate that the failure sequence along the slip surface was similar for the slope with different nail lengths. However, the settlement of the loading plate corresponding to the local failure was evidently smaller if the nail length was reduced. This can explain why the ultimate load pressure of the slope required less settlement of the loading plate when shorter nails were used to reinforce the slope. Such a conclusion about the effect of the nail length on the failure behaviour can be found in the nail-reinforcement design of a slope.

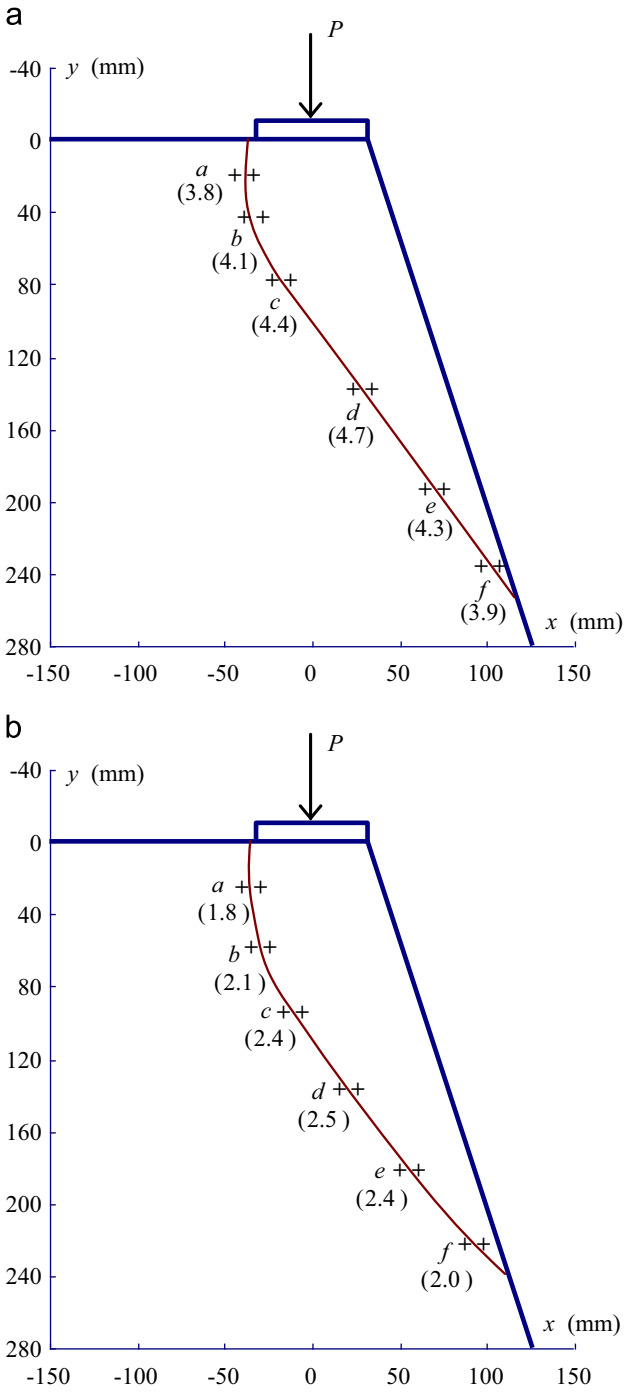

Fig. 8. Development process of slip surface of 3:1 slope with different nail lengths. Numbers in brackets show settlements of loading plate corresponding to appearance of slippage at model dimension (unit: mm). (a) Nail length: 80 mm, (b) Nail length: 50 mm.

5. Deformation behaviour of slope

5.1. Displacement-based analysis

It has been indicated that the settlement of the loading plate on the slope top increased with an increasing load pressure. The displacements of several points on the slope were measured to further understand the deformation behaviour of the slope under a continuous vertical load application (Fig. 9). Both the horizontal and the vertical displacements of all the measurement points increased as the vertical load pressure was increased. The displacement of the measurement points along the axis of the loading plate decreased with an increasing distance from the slope top. The displacement history of the slope can be divided into two stages according to the inflexion on the history curve. The displacement increased slowly with an increasing load pressure in the initial loading stage, and exhibited a rapid increase after the load pressure increased to a value in the rapid development stage. It should be noted that the load pressure of the inflexions was different for different points; this demonstrates that the slope exhibited a distribution in the features of displacement.

Fig. 10 shows the horizontal distribution of the vertical displacement of a 3:1 slope at four elevations when the settlement of the loading plate was 4 mm. The vertical displacement decreased with an increasing distance from the slope top. In the upper part of the slope (e.g., $y=40$ mm and $y=110$ mm), the vertical displacement exhibited a distribution like a saddle, with the maximum near the axis of the loading plate. On the other hand, the vertical displacement increased from the interior of the slope to the slope surface in the lower part of the slope

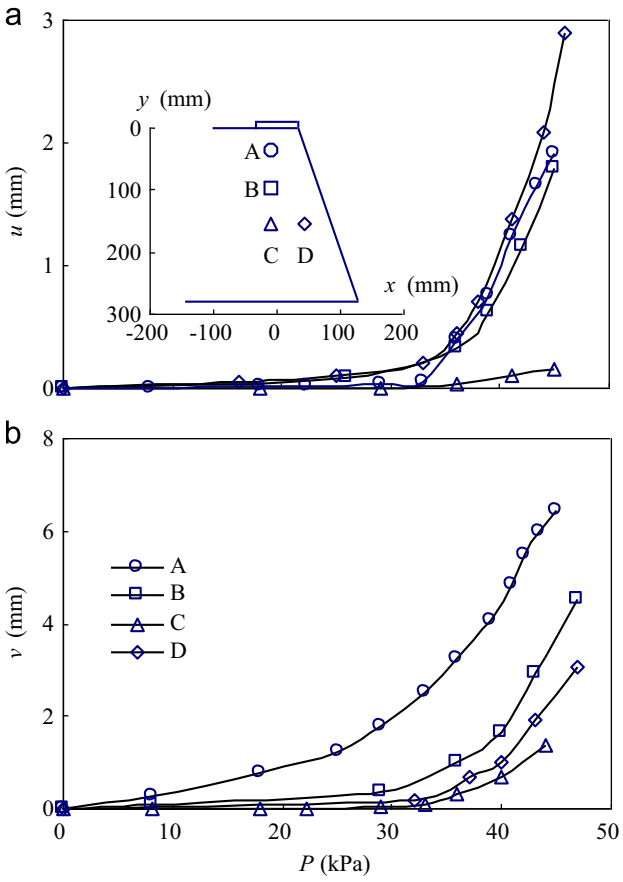

Fig. 9. Displacement histories of typical points of 3:1 slope with nail length of 100 mm at model dimension. P: load pressure on loading plate, u: horizontal displacement, v: vertical displacement. (a) Horizontal displacement and (b) Vertical displacement.

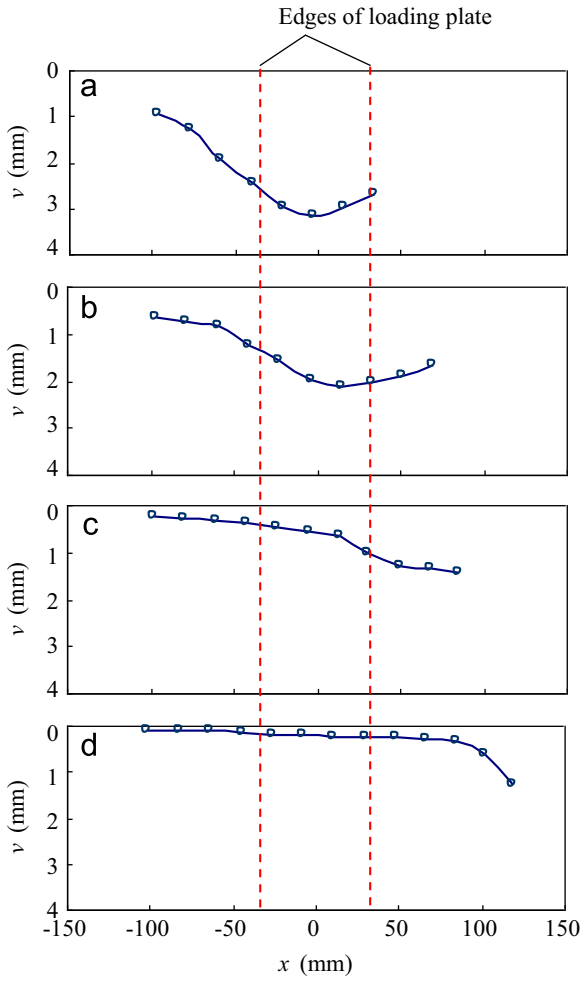

Fig. 10. Horizontal distributions of vertical displacement of 3:1 slope with nail length of 100 mm at 4 mm settlement of loading plate at model dimension. v: vertical displacement, x: horizontal coordinate. (a) $y=40$ mm, (b) $y=110$ mm, (c) $y=180$ mm, and (d) $y=250$ mm.

(e.g., $y=180$ mm and $y=250$ mm). It can be concluded that the distribution feature of the vertical displacement of the slope exhibited an evident change as the distance from the slope top increased.

Fig. 11 summarises the vertical distributions of the location where the peak vertical displacement along a horizontal line of the slopes is in different tests. It can be seen that different slope gradients or different nail lengths yielded similar rules. The peak's position moved from the axis of the loading plate to the slope surface as the distance from the slope top increased for all the slopes. This demonstrated that the application of the surface load was dispersed within the slope. The increase in slope gradient or the decrease in nail length resulted in the decrease in distance from the slope top when the peak's position of the vertical displacement reached the extension line of the outer edge of the loading plate. This indicates that the dispersion of the surface load was accelerated by the increasing slope gradient or the decreasing nail length.

The contour lines of the 1-mm vertical displacement were compared for the slope with different gradients

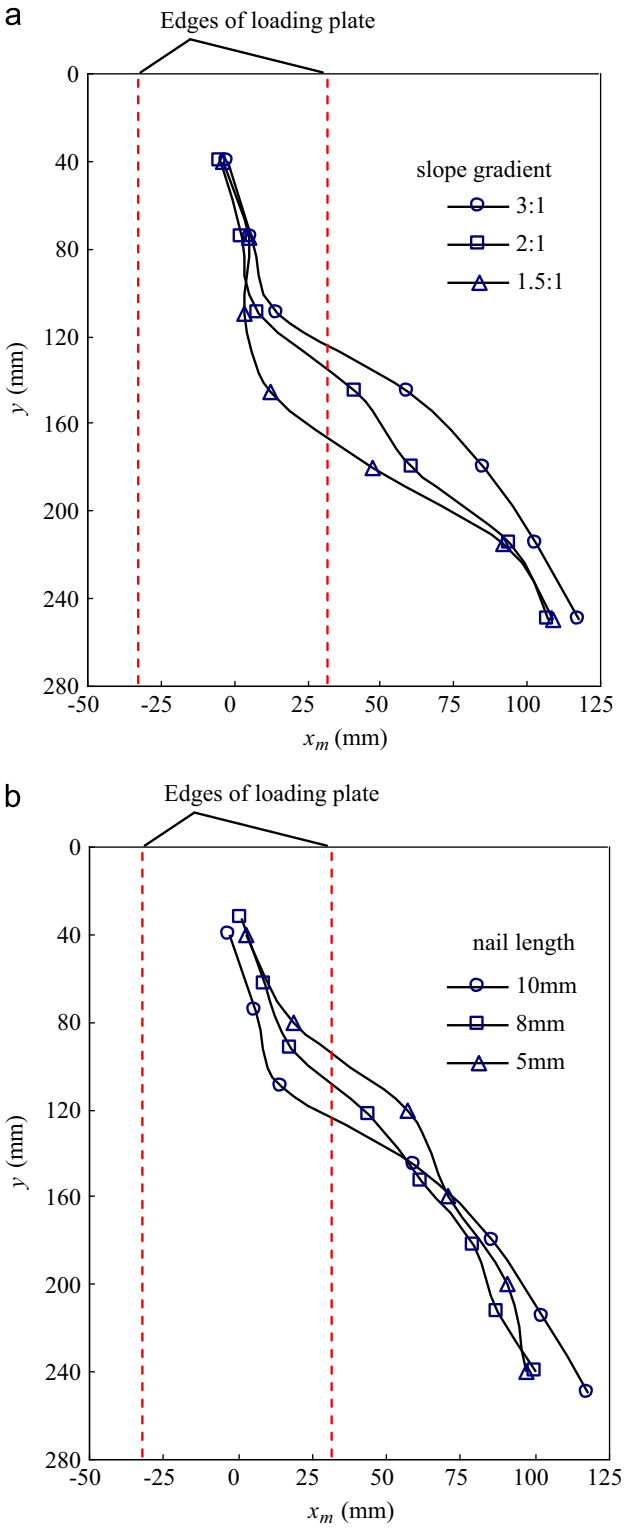

Fig. 11. Positions of peak vertical displacement along horizontal lines of slopes at 4 mm settlement of loading plate at model dimension. x_m: x coordinate of peak vertical displacement along a horizontal line. (a) Slopes with different gradients, (b) 3:1 slope with different nail lengths

(Fig. 12). It should be noted that the boundaries of the measurement zone are outlined using dashed lines due to the requirements of the image-based measurement system. It can be seen that the deformation region extended

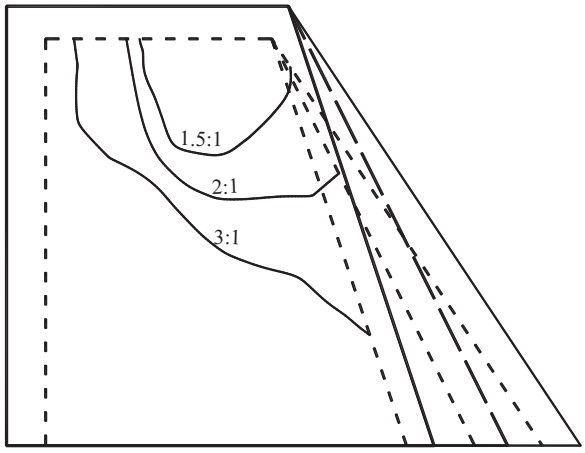

Fig. 12. Vertical displacement contours of 1 mm of slope with different gradients at 4 mm settlement of loading plate at model dimension (nail length: 100 mm).

with an increasing slope gradient. The slope gradient was concluded to have an evident effect on the deformation of the slope.

Close examination of the horizontal distributions of the horizontal displacement showed that the horizontal displacement exhibited an evident increase from nearly zero with a decreasing distance from the slope surface (Fig. 13). However, the locations where the horizontal displacement became visible were different at different locations, indicating that they were dependent on the geometry features of the slope and of the loading plate. Thus, a continuous surface was obtained by connecting the locations where the horizontal displacement became visible to distinguish the zone where the surface load influenced the horizontal displacement of the slope. Such a surface, outlined using the dashed line in Fig. 13, was termed the *H-surface* in this paper.

Fig. 14 shows the *H-surfaces* of the reinforced slope with different slope gradients and different nail lengths. It can be seen that the *H-surface* was behind the inner edge of the loading plate near the slope top and moved to the slope surface with the increasing distance from the slope top. This was consistent with the distribution of the peak vertical displacement along a horizontal line (Fig. 12). The *H-surface* was affected by the slope gradient or the nail length. Since the horizontal displacement is usually regarded as an important sign of the slide failure of a slope, the *H-surface* can be used to direct the reinforcement design of a slope under surface loading conditions. For example, the nail length can be designed according to the *H-surface* in order to achieve a good reinforcement effect, e.g., in view of deformation control.

5.2. Strain-based analysis

The strain of a four-node square element, with a side length of 10 mm, was used to further analyse the deformation behaviour of the slope. The strain of the element can

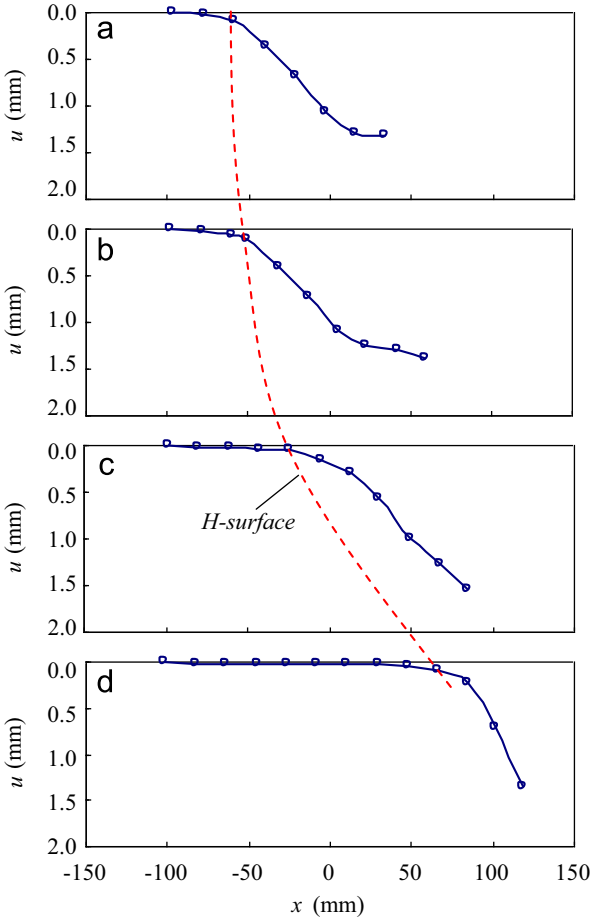

Fig. 13. Horizontal distributions of horizontal displacement of 3:1 slope with nail length of 100 mm at 4 mm settlement of loading plate at model dimension. *u*: horizontal displacement, *x*, horizontal coordinate; *y*, vertical coordinate. (a) $y=40$ mm, (b) $y=110$ mm, (c) $y=180$ mm, and (d) $y=250$ mm.

be obtained through a common isoparametric scheme that was commonly used in the finite element method. It should be noted that the displacement vectors of the nodes were measured using the image-measurement system in the centrifuge model tests.

Four typical elements were picked up within the slope to analyse the strain history (Fig. 15). Three elements were along the axis of the loading plate with different distances from the slope top, and the other element was located near the slip surface. For the element near the slip surface, the slope-direction shear strain increased with an increasing settlement of the loading plate. The shear strain increased rapidly from nearly 4 mm at the settlement of the loading plate, and was fairly large when the slope was nearly destroyed; this demonstrated that a significant shear deformation appeared there. In addition, the volumetric strain exhibited an increasing dilation during loading, with similar change rules as the shear strain.

The volumetric strain along the axis of the loading plate decreased with an increasing distance from the slope top (Fig. 15); this demonstrates that the influence of the vertical load was weakened in the slope. Both the shear strain and the volumetric strain of the element under the

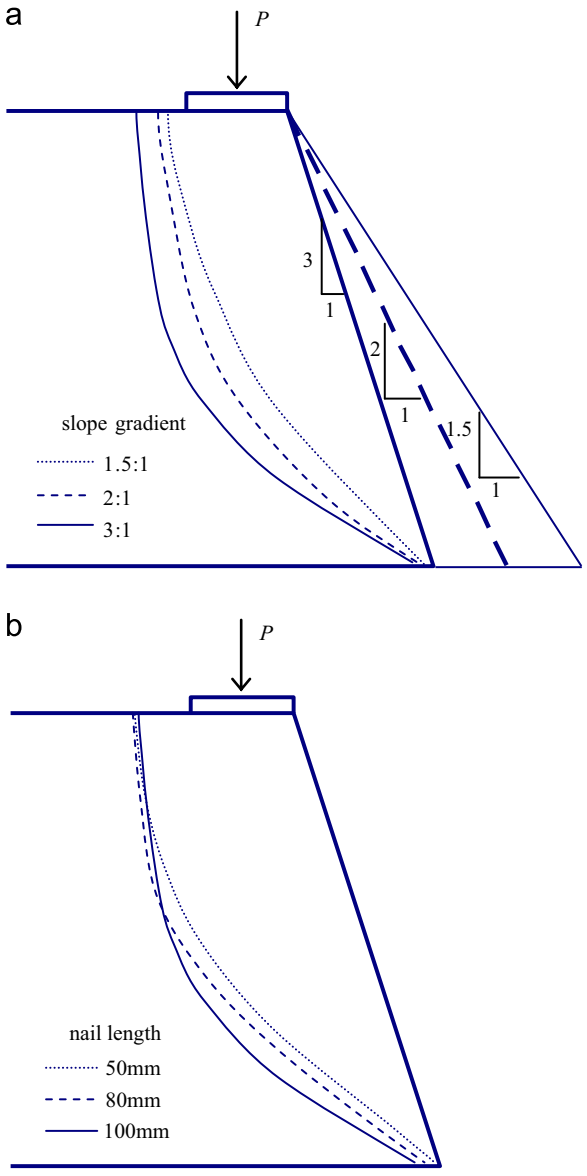

Fig. 14. *H-surfaces* of slopes in different tests. (a) Slopes with different gradients (nail length: 100 mm), (b) 3:1 slope with different nail lengths.

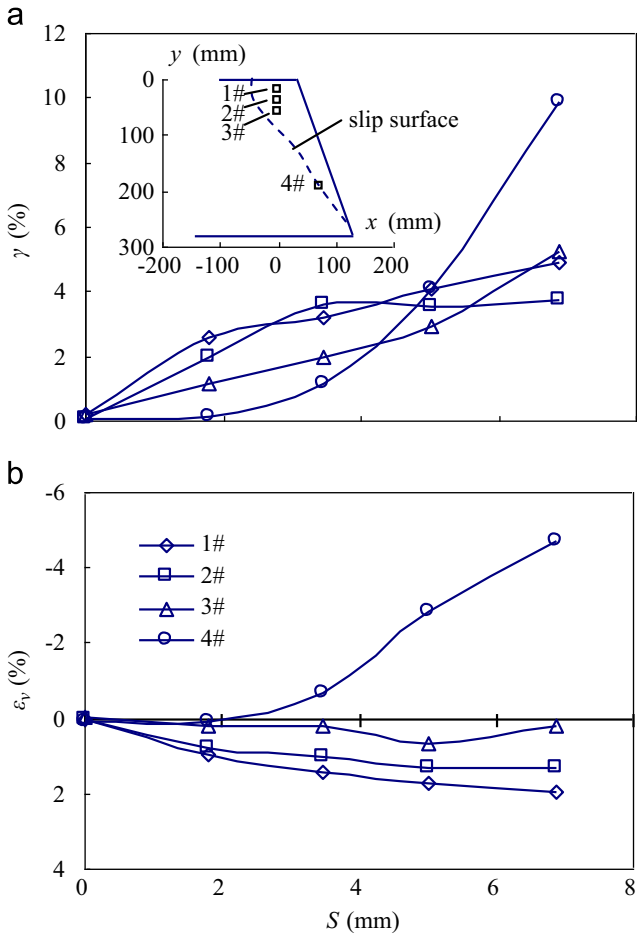

Fig. 15. Strain histories of typical elements of 3:1 slope with nail length of 100 mm. γ: slope-direction shear strain, ε_v: volumetric strain, S: settlement of loading plate. (a) Shear strain, (b) Volumetric strain.

loading plate exhibited a tendency to be stable after the initial increase during loading (Element 1♯ in Fig. 15); this demonstrated that the deformation of the slope under the loading plate was restricted by the loading plate and the nails. It can be concluded that the compression was dominant near the loading plate, and that the compression application was weakened with an increasing distance from the slope top.

6. Response of nails

No tension breakages of nails were discovered according to the examination of the nails in the slope after the tests. It can be inferred that the nails exhibited a pull-out tendency due to the deformation of the surrounding soil. In other words, the nail pull-out failure was dominant according to the centrifuge model tests in this paper, which corresponded to one of the failure modes of the soil nails in practice.

The slope and the inside nails exhibited complicated interaction to provide an overall support against the load, whereas the stress and the deformation of the nails were difficult to measure directly during the tests. The nails exhibited a significant bending deformation because the nails were fairly flexible, which reflected an important aspect of the soil–nail interaction. In this paper, the nails were assumed to bend with the surrounding soil due to the application of the surface load. In other words, the deflections of the nails, perpendicular to the nail length direction, can be obtained from the corresponding deformation of the soil. Thus, the deflections of the nails can be tracked during the whole process of loading using the image-based measurement system.

Such an assumption was verified using the centrifuge model tests on the 3:1 slope with a nail length of 100 mm. Three typical nails were selected in the slope (Fig. 16(a)). The image-based displacement measurement was used to obtain the deflections of these nails. These nails were exposed by peeling away the soil covering them after

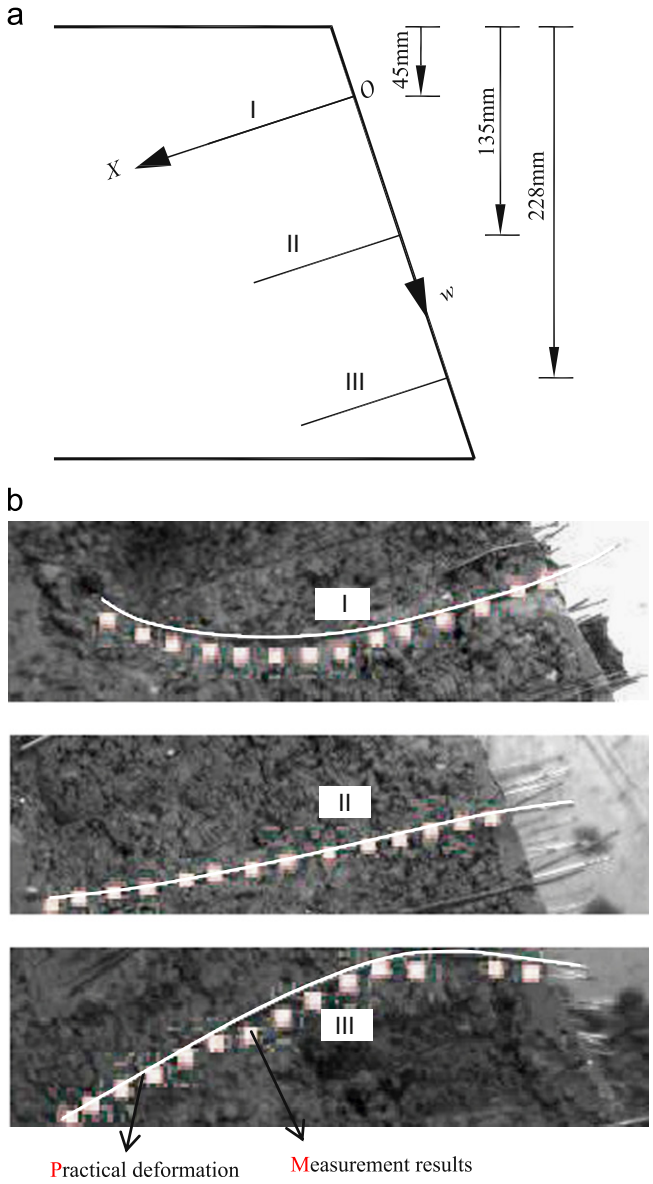

Fig. 16. Deformation of typical nails obtained from measurement system and image of 3:1 slope with nail length of 100 mm after tests. Point: image-measurement results, line: actual shape obtained from image directly. (a) Locations of nails and local coordinates, (b) Results.

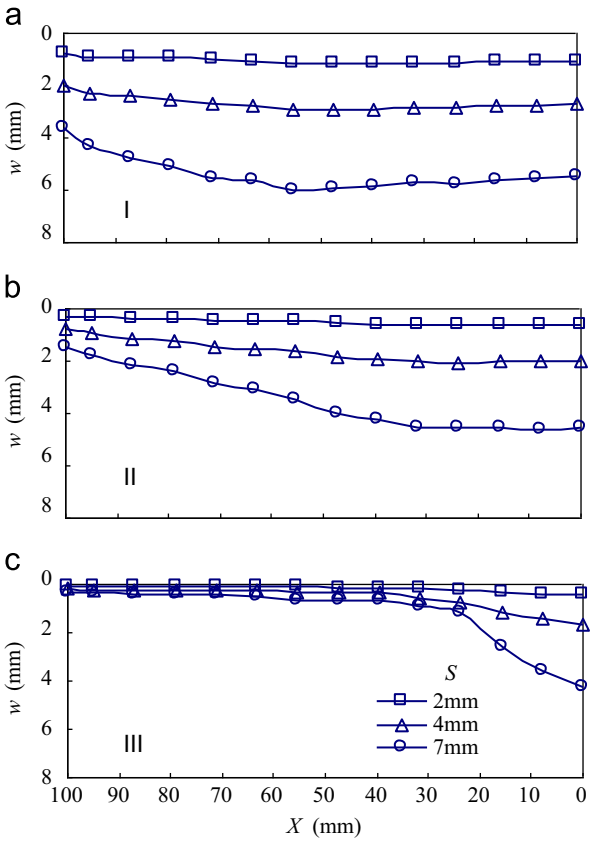

Fig. 17. Distributions of nail deflection of 3:1 slope with nail length of 100 mm at model dimension (locations of nails are shown in Fig. 16(a)). *w*: nail deflection, *X*: distance from slope surface, *S*: settlement of loading plate.

the test, and their deformation was compared with the measurement results (Fig. 16(b)). It can be seen that the measured deflection of the nails were a good fit to the observation of the actual shape of the nails. Thus, the determination method for the deflection of the nails was acceptable.

A local *w*–*X* coordinate system with an origin at the intersection between the nail and the slope surface was set up on the nail to describe the deformation of it, and the *X*-axis and the *w*-axis were parallel to the nail and the slope surface, respectively (Fig. 16(a)). Fig. 17 shows the distributions of the deflections of the three typical nails of a 3:1 slope at different settlements of the loading plate. It can be seen that the deflections of the nails increased with an increasing settlement of the loading plate, indicating that the nail–soil interaction gradually enhanced during loading. In the upper part of the slope, nail I exhibited a nearly parabolic distribution with the maximum in the midpoint (Fig. 17(a)). On the other hand, the deflection of nail III increased from the interior of the slope to the slope surface in the lower part of the slope (Fig. 17(c)). In addition, an inflexion point was discovered near the slope surface owing to the progressive formation of the slip surface (Fig. 4(b)), which indicated a strong interaction between the nail and the neighbouring soil there. The deflection of nail II in the middle of the slope exhibited a linear distribution in the interior of the slope and became nearly stable near the slope surface (Fig. 17(b)). In summary, the nails exhibited diverse features in the deflection distribution in different areas of the slope; this indicates that the soil–nail interaction exhibited a distinction between the areas.

The maximum deflection of a nail in the middle of the slope was examined according to different slope gradients (Fig. 18). It can be seen that the maximum nail deflection increased with an increasing slope gradient, and also increased as the settlement of the loading plate was raised for all the slopes. This suggests that the slope gradient had a positive effect on the soil–nail interaction.

It should be noted that the effectiveness of the proposed determination method of nail deflection should be verified

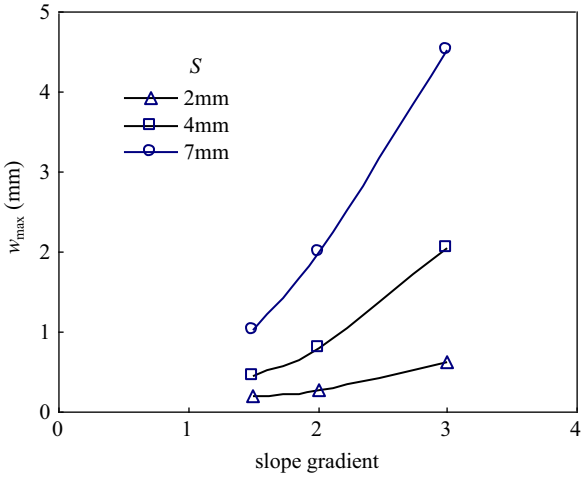

Fig. 18. Maximal deflection of soil nails II of slopes with different gradients at model dimension (nail length: 100 mm). w_{max}: maximum deflection of nail, S: settlement of loading plate.

under different conditions, such as different soil properties of the slope or different reinforcement spacings. For example, it can be imagined that the nails and the surrounding soil may exhibit evidently different movement if the reinforcement spacing is increased to a large magnitude.

7. Conclusions

Based on the observation and the measurement results of a series of centrifuge model tests on a nail-reinforced slope under vertical surface loading conditions, the main conclusions can be drawn as follows:

(1) The vertical load pressure at the top of the slope increased with a decreased rate as the settlement of the loading plate was increased, and exhibited a peak value when the nails were short, while it became nearly stable when the nails were long. The ultimate load of the slope increased significantly with an increasing nail length or a decreasing gradient of the slope.

(2) The slope exhibited significant progressive failure that was captured on the basis of a displacement-based analysis. The vertical load firstly caused local slippage near the slope toe and the inner edge of the loading plate, which then extended to the interior of the slope and eventually developed into an entire slip surface.

(3) The *H-surface* was obtained by connecting the locations where the horizontal displacement had become visible to distinguish the zone in which the surface load had influenced the horizontal displacement of the slope. The *H-surface* and the deformation of the slope were both affected by the slope gradient and the nail length.

(4) The *H-surface* and the position where the peak vertical displacement occurred in a horizontal line moved from the internal slope to the slope surface from the slope top to the slope bottom. This demonstrates the dispersion of the surface load application within the slope.

(5) The deflections of the nails can be obtained from the corresponding deformation of the soil. The maximum deflection of the nails occurred at their midpoint in the upper part of the slope and occurred near the slope surface in the lower part of the slope.

Acknowledgements

The study was supported by the National Natural Science Foundation of China (No. 51079073, 50979045).

References

Alamshahi, S., Hataf, N., 2009. Bearing capacity of strip footings on sand slopes reinforced with geogrid and grid-anchor. Geotextiles and Geomembranes 27, 217–226.

Andrzej, S., Danuta, L., Marek, K., 1988. Measured and predicted stresses and bearing capacity of a full scale slope reinforced with nails. Soils and Foundations 28 (4), 47–56.

El Sawwaf, M.A., 2005. Strip footing behavior on pile and sheet pile-stabilized sand slope. Journal of Geotechnical and Geoenvironmental Engineering 131 (6), 705–715.

Gui, M.W., Ng, C.W.W., 2006. Numerical study of a nailed slope excavation. Geotechnical Engineering 37 (1), 1–12.

Guler, E., Bozkurt, C.F., 2004. The effect of upward nail inclination to the stability of soil nailed structures. Geotechnical Special Publication ASCE 126, 2213–2220.

Hu, Y., Zhang, G., Zhang, J.M., Lee, C.F., 2010. Centrifuge modeling of geotextile-reinforced cohesive slopes. Geotextiles and Geomembranes 28 (1), 12–22.

Juran, I., Baudrand, G., Farrag, K., Elias, V., 1990. Kinematical limit analysis of soil–nailed structures. Journal of Geotechnical Division ASCE 116 (1), 54–73.

Kim, J.S., Kim, J.Y., Lee, S.R., 1997. Analysis of soil nailed earth slope by discrete element method. Computers and Geotechnics 20 (1), 1–14.

Lee, K.M., Manjunath, V.R., 2000. Experimental and numerical studies of geosynthetic-reinforced sand slopes loaded with a footing. Canadian Geotechincal Journal 37 (4), 828–842.

Nowatzki, E., Samtani, N., 2004. Design, construction, and performance of an 18-m soil nail wall in Tucson, AZ. Geotechnical Special Publication ASCE 124, 741–752.

Shen, C.K., Bang, S., Hermann, L.R., 1981. Ground movement and analysis of earth support system. Journal of Geotechnical Division ASCE 107 (12), 1609–1624.

Sommers, A.N., Viswanadham, B.V.S., 2009. Centrifuge model tests on the behavior of strip footing on geotextile-reinforced slopes. Geotextiles and Geomembranes 27, 497–505.

Turner, J.P., Jensen, W.G., 2005. Landslide stabilization using soil nail and mechanically stabilized earth walls: case study. Journal of Geotechnical and Geoenvironmental Engineering 131 (2), 141–150.

Wang, L.P., Zhang, G., Zhang, J.M., 2010. Nail reinforcement mechanism of cohesive soil slopes under earthquake conditions. Soils and Foundations 50 (4), 459–469.

Wang, L.P., Zhang, G., Zhang, J.M., 2011. Centrifuge model tests of geotextile-reinforced soil embankments during an earthquake. Geotextiles and Geomembranes 29 (3), 222–232.

Yang, M.Z., Drumm, E.C., 2000. Numerical analysis of the load transfer and deformation in a soil nailed slope. Geotechnical Special Publication ASCE 96, 102–116.

Yoo, C., 2001. Laboratory investigation of bearing capacity behavior of strip footing on geogrid-reinforced sand slope. Geotextiles and Geomembranes 19, 279–298.

Zhang, G., Hu, Y., Zhang, J.-M., 2009. New image analysis-based displacement-measurement system for geotechnical centrifuge modeling tests. Measurement 42 (1), 87–96.

Zhang, J., Pu, J., Zhang, M., Qiu, T., 2001. Model tests by centrifuge of soil nail reinforcements. Journal of Testing and Evaluation 29 (4), 315–328.

Zhou, Y.D., Cheuk, C.Y., Tham, L.G., 2009. Numerical modeling of soil nails in loose fill slope under surcharge loading. Computers and Geotechnics 36, 837–850.

Zornberg, J.G., Sitar, N., Mitchell, J.K., 1998. Performance of geosynthetic reinforced slopes at failure. Journal of Geotechnical and Geoenvironmental Engineering 124 (8), 670–683.